5-22-1997

# Differential Cross Sections of $D^{*\pm}$ Photoproduction in ep Collisions at HERA

J. Breitweg
*Argonne National Laboratory*

M. Derrick
*Argonne National Laboratory*

D. Krakauer
*Argonne National Laboratory*

S. Magill
*Argonne National Laboratory*

D. Mikunas
*Argonne National Laboratory*

*See next page for additional authors*

DESY-97-026

# Differential Cross Sections of $D^{*\pm}$ Photoproduction in $ep$ Collisions at HERA

ZEUS Collaboration

**Abstract**

Inclusive photoproduction of $D^{*\pm}$ in $ep$ collisions at HERA has been measured with the ZEUS detector for photon-proton centre of mass energies in the range $115 < W < 280\,\mathrm{GeV}$ and photon virtuality $Q^2 < 4\,\mathrm{GeV}^2$. The cross section $\sigma_{ep\to D^*X}$ integrated over the kinematic region $p_\perp^{D^*} > 3\,\mathrm{GeV}$ and $-1.5 < \eta^{D^*} < 1.0$ is $(10.6 \pm 1.7(stat.)\,^{1.6}_{1.3}\,(syst.))\,\mathrm{nb}$. Differential cross sections as functions of $p_\perp^{D^*}$, $\eta^{D^*}$ and $W$ are given. The data are compared with two next-to-leading order perturbative QCD predictions. For a calculation using a massive charm scheme the predicted cross sections are smaller than the measured ones. A recent calculation using a massless charm scheme is in agreement with the data.

# The ZEUS Collaboration

J. Breitweg, M. Derrick, D. Krakauer, S. Magill, D. Mikunas, B. Musgrave, J. Repond, R. Stanek, R.L. Talaga, R. Yoshida, H. Zhang
*Argonne National Laboratory, Argonne, IL, USA* [p]

M.C.K. Mattingly
*Andrews University, Berrien Springs, MI, USA*

F. Anselmo, P. Antonioli, G. Bari, M. Basile, L. Bellagamba, D. Boscherini, A. Bruni, G. Bruni, G. Cara Romeo, G. Castellini[1], L. Cifarelli[2], F. Cindolo, A. Contin, M. Corradi, I. Gialas[3], P. Giusti, G. Iacobucci, G. Laurenti, G. Levi, A. Margotti, T. Massam, R. Nania, F. Palmonari, S. De Pasquale, A. Pesci, A. Polini, G. Sartorelli, Y. Zamora Garcia[4], A. Zichichi
*University and INFN Bologna, Bologna, Italy* [f]

C. Amelung, A. Bornheim, I. Brock, K. Coböken, J. Crittenden, R. Deffner, M. Eckert, L. Feld[5], M. Grothe, H. Hartmann, K. Heinloth, L. Heinz, E. Hilger, H.-P. Jakob, U.F. Katz, E. Paul, M. Pfeiffer, Ch. Rembser, J. Stamm, R. Wedemeyer[6]
*Physikalisches Institut der Universität Bonn, Bonn, Germany* [c]

D.S. Bailey, S. Campbell-Robson, W.N. Cottingham, B. Foster, R. Hall-Wilton, M.E. Hayes, G.P. Heath, H.F. Heath, D. Piccioni, D.G. Roff, R.J. Tapper
*H.H. Wills Physics Laboratory, University of Bristol, Bristol, U.K.* [o]

M. Arneodo[7], R. Ayad, M. Capua, A. Garfagnini, L. Iannotti, M. Schioppa, G. Susinno
*Calabria University, Physics Dept.and INFN, Cosenza, Italy* [f]

J.Y. Kim, J.H. Lee, I.T. Lim, M.Y. Pac[8]
*Chonnam National University, Kwangju, Korea* [h]

A. Caldwell[9], N. Cartiglia, Z. Jing, W. Liu, J.A. Parsons, S. Ritz[10], S. Sampson, F. Sciulli, P.B. Straub, Q. Zhu
*Columbia University, Nevis Labs., Irvington on Hudson, N.Y., USA* [q]

P. Borzemski, J. Chwastowski, A. Eskreys, Z. Jakubowski, M.B. Przybycień, M. Zachara, L. Zawiejski
*Inst. of Nuclear Physics, Cracow, Poland* [j]

L. Adamczyk, B. Bednarek, K. Jeleń, D. Kisielewska, T. Kowalski, M. Przybycień, E. Rulikowska-Zarębska, L. Suszycki, J. Zając
*Faculty of Physics and Nuclear Techniques, Academy of Mining and Metallurgy, Cracow, Poland* [j]

Z. Duliński, A. Kotański
A. Kotański
*Jagellonian Univ., Dept. of Physics, Cracow, Poland* [k]

G. Abbiendi[11], H. Abramowicz, L.A.T. Bauerdick, U. Behrens, H. Beier, J.K. Bienlein, G. Cases, O. Deppe, K. Desler, G. Drews, D.J. Gilkinson, C. Glasman, P. Göttlicher, J. Große-Knetter, T. Haas, W. Hain, D. Hasell, H. Heßling, Y. Iga, K.F. Johnson[12], M. Kasemann, W. Koch, U. Kötz, H. Kowalski, J. Labs, L. Lindemann, B. Löhr, M. Löwe[13], J. Mainusch[14], O. Mańczak, J. Milewski, T. Monteiro[15], J.S.T. Ng[16], D. Notz, K. Ohrenberg[14], I.H. Park[17], A. Pellegrino, F. Pelucchi, K. Piotrzkowski, M. Roco[18], M. Rohde, J. Roldán, A.A. Savin, U. Schneekloth, W. Schulz[19], F. Selonke, B. Surrow, E. Tassi, T. Voß[20],
D. Westphal, G. Wolf, U. Wollmer, C. Youngman, A.F. Żarnecki, W. Zeuner
*Deutsches Elektronen-Synchrotron DESY, Hamburg, Germany*

B.D. Burow, H.J. Grabosch, A. Meyer, S. Schlenstedt
*DESY-IfH Zeuthen, Zeuthen, Germany*

G. Barbagli, E. Gallo, P. Pelfer
*University and INFN, Florence, Italy* [f]

G. Maccarrone, L. Votano
*INFN, Laboratori Nazionali di Frascati, Frascati, Italy* [f]

A. Bamberger, S. Eisenhardt, P. Markun, T. Trefzger[21], S. Wölfle
*Fakultät für Physik der Universität Freiburg i.Br., Freiburg i.Br., Germany* [c]

J.T. Bromley, N.H. Brook, P.J. Bussey, A.T. Doyle, D.H. Saxon, L.E. Sinclair, E. Strickland, M.L. Utley[22], R. Waugh, A.S. Wilson
*Dept. of Physics and Astronomy, University of Glasgow, Glasgow, U.K.* [o]

I. Bohnet, N. Gendner, U. Holm, A. Meyer-Larsen, H. Salehi, K. Wick
*Hamburg University, I. Institute of Exp. Physics, Hamburg, Germany* [c]

L.K. Gladilin[23], R. Klanner, E. Lohrmann, G. Poelz, W. Schott[24], F. Zetsche
*Hamburg University, II. Institute of Exp. Physics, Hamburg, Germany* [c]

T.C. Bacon, I. Butterworth, J.E. Cole, V.L. Harris, G. Howell, B.H.Y. Hung, L. Lamberti[25], K.R. Long, D.B. Miller, N. Pavel, A. Prinias[26], J.K. Sedgbeer, D. Sideris, A.F. Whitfield[27]
*Imperial College London, High Energy Nuclear Physics Group, London, U.K.* [o]

U. Mallik, S.M. Wang, J.T. Wu
*University of Iowa, Physics and Astronomy Dept., Iowa City, USA* [p]

P. Cloth, D. Filges
*Forschungszentrum Jülich, Institut für Kernphysik, Jülich, Germany*

S.H. An, S.B. Lee, S.W. Nam, H.S. Park, S.K. Park
*Korea University, Seoul, Korea* [h]

F. Barreiro, J.P. Fernandez, R. Graciani, J.M. Hernández, L. Hervás, L. Labarga, M. Martinez, J. del Peso, J. Puga, J. Terron, J.F. de Trocóniz
*Univer. Autónoma Madrid, Depto de Física Teóríca, Madrid, Spain* [n]

F. Corriveau, D.S. Hanna, J. Hartmann, L.W. Hung, J.N. Lim, W.N. Murray, A. Ochs, M. Riveline, D.G. Stairs, M. St-Laurent, R. Ullmann
*McGill University, Dept. of Physics, Montréal, Québec, Canada* [a], [b]

T. Tsurugai
*Meiji Gakuin University, Faculty of General Education, Yokohama, Japan*

V. Bashkirov, B.A. Dolgoshein, A. Stifutkin
*Moscow Engineering Physics Institute, Mosocw, Russia* [l]

G.L. Bashindzhagyan, P.F. Ermolov, Yu.A. Golubkov, V.D. Kobrin, I.A. Korzhavina, V.A. Kuzmin, O.Yu. Lukina, A.S. Proskuryakov, L.M. Shcheglova, A.N. Solomin, N.P. Zotov
*Moscow State University, Institute of Nuclear Physics, Moscow, Russia* [m]

C. Bokel, M. Botje, N. Brümmer, F. Chlebana[18], J. Engelen, M. de Kamps, P. Kooijman, A. Kruse, A. van Sighem, H. Tiecke, W. Verkerke, J. Vossebeld, M. Vreeswijk, L. Wiggers, E. de Wolf
*NIKHEF and University of Amsterdam, Netherlands* [i]

D. Acosta, B. Bylsma, L.S. Durkin, J. Gilmore, C.M. Ginsburg, C.L. Kim, T.Y. Ling, P. Nylander, T.A. Romanowski[28]
*Ohio State University, Physics Department, Columbus, Ohio, USA* [p]

H.E. Blaikley, R.J. Cashmore, A.M. Cooper-Sarkar, R.C.E. Devenish, J.K. Edmonds, N. Harnew, M. Lancaster[29], J.D. McFall, C. Nath, V.A. Noyes[26], A. Quadt, J.R. Tickner, H. Uijterwaal, R. Walczak, D.S. Waters, T. Yip
*Department of Physics, University of Oxford, Oxford, U.K.* [o]

A. Bertolin, R. Brugnera, R. Carlin, F. Dal Corso, U. Dosselli, S. Limentani, M. Morandin, M. Posocco, L. Stanco, R. Stroili, C. Voci
*Dipartimento di Fisica dell' Universita and INFN, Padova, Italy* [f]

J. Bulmahn, R.G. Feild[30], B.Y. Oh, J.R. Okrasiński, J.J. Whitmore
*Pennsylvania State University, Dept. of Physics, University Park, PA, USA* [q]

G. D'Agostini, G. Marini, A. Nigro
*Dipartimento di Fisica, Univ. 'La Sapienza' and INFN, Rome, Italy* [f]

J.C. Hart, N.A. McCubbin, T.P. Shah
*Rutherford Appleton Laboratory, Chilton, Didcot, Oxon, U.K.* [o]

E. Barberis[29], T. Dubbs, C. Heusch, M. Van Hook, W. Lockman, J.T. Rahn, H.F.-W. Sadrozinski, A. Seiden, D.C. Williams
*University of California, Santa Cruz, CA, USA* [p]

O. Schwarzer, A.H. Walenta
*Fachbereich Physik der Universität-Gesamthochschule Siegen, Germany* [c]

G. Briskin, S. Dagan[31], T. Doeker, A. Levy[32]
*Raymond and Beverly Sackler Faculty of Exact Sciences, School of Physics, Tel-Aviv University, Tel-Aviv, Israel* [e]

T. Abe, J.I. Fleck[33], M. Inuzuka, T. Ishii, M. Kuze, K. Nagano, M. Nakao, I. Suzuki, K. Tokushuku, K. Umemori, S. Yamada, Y. Yamazaki
*Institute for Nuclear Study, University of Tokyo, Tokyo, Japan* [g]

R. Hamatsu, T. Hirose, K. Homma, S. Kitamura[34], T. Matsushita, K. Yamauchi
*Tokyo Metropolitan University, Dept. of Physics, Tokyo, Japan* [g]

R. Cirio, M. Costa, M.I. Ferrero, S. Maselli, V. Monaco, C. Peroni, M.C. Petrucci, R. Sacchi, A. Solano, A. Staiano
*Universita di Torino, Dipartimento di Fisica Sperimentale and INFN, Torino, Italy* [f]

M. Dardo
*II Faculty of Sciences, Torino University and INFN - Alessandria, Italy* [f]

D.C. Bailey, M. Brkic, C.-P. Fagerstroem, G.F. Hartner, K.K. Joo, G.M. Levman, J.F. Martin, R.S. Orr, S. Polenz, C.R. Sampson, D. Simmons, R.J. Teuscher[33]
*University of Toronto, Dept. of Physics, Toronto, Ont., Canada* [a]

J.M. Butterworth, C.D. Catterall, T.W. Jones, P.B. Kaziewicz, J.B. Lane, R.L. Saunders, J. Shulman, M.R. Sutton
*University College London, Physics and Astronomy Dept., London, U.K.* [o]

B. Lu, L.W. Mo
*Virginia Polytechnic Inst. and State University, Physics Dept., Blacksburg, VA, USA* [q]

J. Ciborowski, G. Grzelak[35], M. Kasprzak, K. Muchorowski[36], R.J. Nowak, J.M. Pawlak, R. Pawlak, T. Tymieniecka, A.K. Wróblewski, J.A. Zakrzewski
*Warsaw University, Institute of Experimental Physics, Warsaw, Poland* [j]

M. Adamus
*Institute for Nuclear Studies, Warsaw, Poland* [j]

C. Coldewey, Y. Eisenberg[31], D. Hochman, U. Karshon[31], D. Revel[31], D. Zer-Zion
*Weizmann Institute, Nuclear Physics Dept., Rehovot, Israel* [d]

W.F. Badgett, D. Chapin, R. Cross, S. Dasu, C. Foudas, R.J. Loveless, S. Mattingly, D.D. Reeder, W.H. Smith, A. Vaiciulis, M. Wodarczyk
*University of Wisconsin, Dept. of Physics, Madison, WI, USA* [p]

S. Bhadra, W.R. Frisken, M. Khakzad, W.B. Schmidke
*York University, Dept. of Physics, North York, Ont., Canada* [a]

[1] also at IROE Florence, Italy
[2] now at Univ. of Salerno and INFN Napoli, Italy
[3] now at Univ. of Crete, Greece
[4] supported by Worldlab, Lausanne, Switzerland
[5] now OPAL
[6] retired
[7] also at University of Torino and Alexander von Humboldt Fellow
[8] now at Dongshin University, Naju, Korea
[9] also at DESY and Alexander von Humboldt Fellow
[10] Alfred P. Sloan Foundation Fellow
[11] supported by an EC fellowship number ERBFMBICT 950172
[12] visitor from Florida State University
[13] now at ALCATEL Mobile Communication GmbH, Stuttgart
[14] now at DESY Computer Center
[15] supported by European Community Program PRAXIS XXI
[16] now at DESY-Group FDET
[17] visitor from Kyungpook National University, Taegu, Korea, partially supported by DESY
[18] now at Fermi National Accelerator Laboratory (FNAL), Batavia, IL, USA
[19] now at Siemens A.G., Munich
[20] now at NORCOM Infosystems, Hamburg
[21] now at ATLAS Collaboration, Univ. of Munich
[22] now at Clinical Operational Research Unit, University College, London
[23] on leave from MSU, supported by the GIF, contract I-0444-176.07/95
[24] now a self-employed consultant
[25] supported by an EC fellowship
[26] PPARC Post-doctoral Fellow
[27] now at Conduit Communications Ltd., London, U.K.
[28] now at Department of Energy, Washington
[29] now at Lawrence Berkeley Laboratory, Berkeley
[30] now at Yale University, New Haven, CT
[31] supported by a MINERVA Fellowship
[32] partially supported by DESY
[33] now at CERN
[34] present address: Tokyo Metropolitan College of Allied Medical Sciences, Tokyo 116, Japan
[35] supported by the Polish State Committee for Scientific Research, grant No. 2P03B09308
[36] supported by the Polish State Committee for Scientific Research, grant No. 2P03B09208

[a] supported by the Natural Sciences and Engineering Research Council of Canada (NSERC)
[b] supported by the FCAR of Québec, Canada
[c] supported by the German Federal Ministry for Education and Science, Research and Technology (BMBF), under contract numbers 057BN19P, 057FR19P, 057HH19P, 057HH29P, 057SI75I
[d] supported by the MINERVA Gesellschaft für Forschung GmbH, the German Israeli Foundation, and the U.S.-Israel Binational Science Foundation
[e] supported by the German Israeli Foundation, and by the Israel Academy of Science
[f] supported by the Italian National Institute for Nuclear Physics (INFN)
[g] supported by the Japanese Ministry of Education, Science and Culture (the Monbusho) and its grants for Scientific Research
[h] supported by the Korean Ministry of Education and Korea Science and Engineering Foundation
[i] supported by the Netherlands Foundation for Research on Matter (FOM)
[j] supported by the Polish State Committee for Scientific Research, grant No. 115/E-343/SPUB/P03/120/96
[k] supported by the Polish State Committee for Scientific Research (grant No. 2 P03B 083 08) and Foundation for Polish-German Collaboration
[l] partially supported by the German Federal Ministry for Education and Science, Research and Technology (BMBF)
[m] supported by the German Federal Ministry for Education and Science, Research and Technology (BMBF), and the Fund of Fundamental Research of Russian Ministry of Science and Education and by INTAS-Grant No. 93-63
[n] supported by the Spanish Ministry of Education and Science through funds provided by CICYT
[o] supported by the Particle Physics and Astronomy Research Council
[p] supported by the US Department of Energy
[q] supported by the US National Science Foundation

# 1 Introduction

Production of the heavy quarks $c$ and $b$ at HERA is dominated by photoproduction, where a quasi-real photon with negative four momentum squared, $Q^2$, close to zero is emitted by the incoming electron and interacts with the proton. Heavy quark photoproduction can be used to probe perturbative QCD calculations with a hard scale stemming from the heavy quark mass and the high transverse momentum of the produced parton. At leading order (LO) in QCD two types of processes are responsible for the production of heavy quarks: the direct photon processes, where the photon participates as a point-like particle which interacts with a parton from the incoming proton, and the resolved photon processes, where the photon is a source of partons, one of which scatters off a parton from the proton. Charm quarks present in the parton distributions of the photon, as well as of the proton, lead to processes like $cg \to cg$, which are called charm flavour excitation. In next-to-leading order (NLO) QCD only the sum of direct and resolved processes is unambiguously defined. Two types of NLO calculations using different approaches are available for comparison with measurements of charm photoproduction at HERA. The massive charm approach [1, 2, 3] assumes light quarks to be the only active flavours within the structure functions of the proton and the photon, while the massless charm approach [4, 5] also treats charm as an active flavour.

The total charm photoproduction cross section $\sigma_{\gamma p \to c\bar{c}X}$ has recently been measured at HERA [6, 7] at a $\gamma p$ centre of mass energy $W \approx 200\,\mathrm{GeV}$, and was found to be about one order of magnitude larger than fixed target data. These measurements were compared with NLO QCD calculations [2] and with a calculation based on a semihard approach of QCD [8]. The precision of the comparison was limited by large systematic uncertainties in both data and theory. In the case of the data the uncertainty was due to the necessity of extrapolating the measured cross sections into kinematic regions not accessible to the experiments. The uncertainties of the theoretical predictions were generated by the dependence of the NLO calculations on the charm mass, $m_c$, the QCD renormalization and factorization scales, and on the parton density parametrizations assumed for the proton and the photon.

In this study we use a sample of $D^*(2010)^{\pm}$ mesons collected with the ZEUS detector during 1994. The sixfold increase of the data sample with respect to our previous analysis [6] allowed the measurement of the differential distributions in $p_\perp^{D^*}$, $\eta^{D^*}$ and $W$, where $p_\perp^{D^*}$ is the $D^*$ transverse momentum with respect to the beam axis and $\eta^{D^*}$ is the pseudorapidity[1] of the $D^*$. The measurement of the $ep \to D^*X$ cross sections was performed in the restricted kinematic region $Q^2 < 4\,\mathrm{GeV}^2$, $115 < W < 280\,\mathrm{GeV}$, $p_\perp^{D^*} > 3\,\mathrm{GeV}$ and $-1.5 < \eta^{D^*} < 1.0$. The results are compared with NLO QCD predictions calculated in both the massive and the massless charm approach. The theoretical uncertainties in the calculations are strongly reduced in the restricted kinematic region, thus allowing a more precise comparison of the perturbative QCD calculations with our data. The results of

[1] The pseudorapidity $\eta$ is defined as $-\ln(\tan\frac{\theta}{2})$, where the polar angle $\theta$ is taken with respect to the proton beam direction.

the calculations using a massless charm scheme are sensitive to the charm content of the photon and are insensitive to that of the proton [4, 9].

$D^*$ mesons are reconstructed from their decay products through the two decay modes[2]:

$$D^{*+} \to D^0 \pi_S^+ \to (K^- \pi^+) \pi_S^+, \tag{1}$$

$$D^{*+} \to D^0 \pi_S^+ \to (K^- \pi^+ \pi^+ \pi^-) \pi_S^+. \tag{2}$$

The small mass difference $M(D^*) - M(D^0) = 145.42 \pm 0.05\,\mathrm{MeV}$ [10] yields a low momentum pion ("soft pion", $\pi_S$) from the $D^*$ decay and prominent signals just above the threshold of the $M(K\pi\pi_S) - M(K\pi)$ and $M(K\pi\pi\pi\pi_S) - M(K\pi\pi\pi)$ distributions, where the phase space contribution is highly suppressed [11].

# 2 Experimental Conditions

The data presented in this analysis were collected during the 1994 running period using the ZEUS detector at HERA, where a positron beam with energy $E_e = 27.5\,\mathrm{GeV}$ collided with a proton beam with energy $E_p = 820\,\mathrm{GeV}$. A total of 153 colliding bunches were stored in HERA, together with additional 17 proton and 15 positron unpaired bunches intended for studies of beam-induced backgrounds. The time interval between bunch crossings was 96 ns, and the typical instantaneous luminosity was $1.5{\cdot}10^{30}\,\mathrm{cm}^{-2}\mathrm{s}^{-1}$. The r.m.s. of the vertex position distribution along the beam direction was 12 cm. The total integrated luminosity used in this analysis is $2.99\,\mathrm{pb}^{-1}$.

## 2.1 The ZEUS Detector

A detailed description of the ZEUS detector can be found in ref. [12, 13]. Here we present a brief description of the components relevant to the present analysis.

Charged particles are measured by the Central Tracking Detector (CTD) [14] which operates in a magnetic field of 1.43 T provided by a thin superconducting solenoid. The CTD is a drift chamber consisting of 72 cylindrical layers, arranged in 9 superlayers. Superlayers with wires parallel to the beam axis alternate with those inclined at a small angle to give a stereo view. The single hit efficiency of the CTD is greater than 95% and the measured resolution in transverse momentum for tracks with hits in all the superlayers is $\sigma_{p_\perp}/p_\perp = 0.005 p_\perp \oplus 0.016$ ($p_\perp$ in GeV).

Surrounding the solenoid is the uranium-scintillator calorimeter (CAL) [15], which is divided into three parts: forward,[3] barrel and rear covering the polar regions 2.6° to

[2] In this analysis the charge conjugated processes are also included.

[3] Throughout this paper we use the standard ZEUS right-handed coordinate system, in which $X = Y = Z = 0$ is the nominal interaction point, the positive $Z$-axis points in the direction of the protons (referred to as the forward direction) and the $X$-axis is horizontal, pointing towards the centre of HERA.

36.7°, 36.7° to 129.1° and 129.1° to 176.2°, respectively. The CAL covers 99.7% of the solid angle, with holes of $20 \times 20$ cm$^2$ in the centres of the forward and rear calorimeters to accommodate the HERA beam pipe. Each of the calorimeter parts is subdivided into towers which are segmented longitudinally into electromagnetic (EMC) and hadronic (HAC) sections. These sections are further subdivided into cells each of which is read out by two photomultipliers. From test beam data, energy resolutions of $\sigma_E/E = 0.18/\sqrt{E}$ for electrons and $\sigma_E/E = 0.35/\sqrt{E}$ for hadrons ($E$ in GeV) have been obtained. The timing resolution of a calorimeter cell is less than 1 ns for energy deposits greater than 4.5 GeV. In order to minimise the effects of noise due to the uranium radioactivity on the measurements, all EMC (HAC) cells with an energy deposit of less than 60 (110) MeV are discarded from the analysis. For cells without energy deposits in neighbouring cells this cut was increased to 80 (120) MeV.

Proton-gas events occurring in front of the nominal $ep$ interaction region are out of time with respect to the $ep$ interactions and may thus be rejected by timing measurements made by the CAL and by scintillation veto counter arrays located at $Z = -730$ cm, $Z = -315$ cm and $Z = -150$ cm.

The luminosity was determined from the rate of the Bethe-Heitler process $e^+p \to e^+\gamma p$, where the photon is measured by a calorimeter [16] located at $Z = -107$ m in the HERA tunnel in the direction of the positron beam.

## 2.2 Trigger

The ZEUS detector uses a three level trigger system [12]. For the analysis presented in this paper the following trigger strategy was chosen to identify $D^*$ candidates in the central region of the detector.

In the first level trigger the calorimeter cells were combined to define regional and global sums which were required to exceed one of the following thresholds:

- Total energy greater than 15 GeV,
- Total EMC energy greater than 10 GeV,
- Total transverse energy greater than 11 GeV,
- EMC energy in the barrel calorimeter greater than 3.5 GeV,
- EMC energy in the rear calorimeter greater than 2 GeV.

In addition, at least one CTD track coming from the $ep$ interaction region was required. Events with timing measured by the veto counters, inconsistent with an $ep$ interaction, were removed.

In the second level trigger beam-gas events were rejected by exploiting the excellent timing resolution of the calorimeter. Also events were rejected in which the vertex determined by the CTD was not compatible with the nominal $ep$ interaction region.

In the third level trigger (TLT) the full event information was available. Calorimeter timing cuts were tightened for further rejection of the remaining beam-gas events. Events were required to have a transverse energy outside a cone of $\theta = 10^\circ$ with respect to the proton direction, $E_\perp^{\theta>10^\circ}$, above 12 GeV. The online value overestimates the offline $E_\perp^{\theta>10^\circ}$ due to the simplified event reconstruction at the TLT. In addition, the following requirements were made:

- $p_\perp^{max+} > 0.5\,\mathrm{GeV}$,
- $p_\perp^{max-} > 0.5\,\mathrm{GeV}$ and
- $p_\perp^{max+} + p_\perp^{max-} > 2.0\,\mathrm{GeV}$,

where the quantity $p_\perp^{max+}$ ($p_\perp^{max-}$) is defined as the maximum transverse momentum of any positive (negative) track associated with the reconstructed event vertex in the polar angle range $15^\circ < \theta < 165^\circ$.

# 3 Data Analysis

## 3.1 Offline Data Selection

The event sample accepted by the trigger algorithm was processed using the standard offline ZEUS detector calibration and event reconstruction code. To define an inclusive photoproduction sample, the following requirements were imposed:

- A reconstructed vertex with at least three tracks associated to it.
- $E_\perp^{\theta>10^\circ} > 12\,\mathrm{GeV}$.
- No scattered positron found in the CAL according to the algorithm described in ref. [17]. This requirement removes deep inelastic scattering (DIS) neutral current events, thereby restricting $Q^2$ to below $4\,\mathrm{GeV}^2$. The corresponding median $Q^2$ is about $5{\cdot}10^{-4}\,\mathrm{GeV}^2$.
- $0.1 < y_{\mathsf{JB}} < 0.7$. Here $y_{\mathsf{JB}}$ is the Jacquet-Blondel [18] estimate of $y$, the fraction of the positron energy carried by the photon in the proton rest frame. It is defined as:

$$y_{\mathsf{JB}} = \frac{\Sigma_i (E - p_z)_i}{2E_e},$$

where the sum runs over all calorimeter cells and $p_z$ is the $Z$ component of the momentum vector assigned to each cell of energy $E$. The lower $y_{\mathsf{JB}}$ cut rejects events from a region where the acceptance is small because of the trigger requirements. The upper cut rejects possible background from DIS events in which the scattered positron has not been identified, and therefore is included in the $y_{\mathsf{JB}}$ calculation, thus producing a value of $y_{\mathsf{JB}}$ closer to 1.

With these requirements, an inclusive photoproduction sample of about 450,000 events was selected. The $\gamma p$ centre of mass energy of these events was calculated from $y_{\mathsf{JB}}$ via the expression $W_{\mathsf{JB}} = \sqrt{4 y_{\mathsf{JB}} E_p E_e}$ and ranges from 100 to 250 GeV. A systematic shift observed in the reconstructed values of $W_{\mathsf{JB}}$ with respect to the true $W$ of the event, due to energy losses in inactive material in front of the calorimeter and particles lost in the rear beam pipe, was corrected using Monte Carlo (MC) techniques [6, 17]. The centre of mass energy range covered by the photoproduction sample is then $115 < W < 280$ GeV.

A $D^*$ reconstruction algorithm was applied to all selected events. This algorithm combines the reconstructed tracks in each event to form $D^*$ candidates assuming the decay channels (1) or (2). It uses the mass difference technique to suppress the high background due to random combinations from non-$c\bar{c}$ events, which have a much higher cross section. Only tracks associated with the event vertex and having $p_\perp > 0.2$ GeV and $|\eta| < 1.75$ are included in the combinations.

## 3.2 The $D^{*+} \to D^0 \pi_S^+ \to (K^- \pi^+) \pi_S^+$ Decay Channel

In each event tracks with opposite charges and $p_\perp > 0.5$ GeV were combined into pairs to form $D^0$ candidates. The invariant mass $M(K\pi)$ of each pair was calculated. No particle identification was used, so kaon and pion masses were assumed in turn for each particle in the pair. A third track, assumed to be the soft pion, $\pi_S$, with a charge opposite to that of the particle taken as a kaon, was then added to the combination. The mass difference $\Delta M = M(K\pi\pi_S) - M(K\pi)$ was evaluated. Only $K\pi\pi_S$ combinations with $-1.5 < \eta < 1.0$, for which the acceptance is high, were kept. As a result of the $E_\perp^{\theta > 10^\circ} > 12$ GeV cut the acceptance of the $K\pi\pi_S$ combinations having $p_\perp$ below 3 GeV is very small. Thus $p_\perp(K\pi\pi_S) > 3$ GeV was required. This cut excludes almost all soft pions with $p_\perp(\pi_S) < 0.2$ GeV, so the overall cut of $p_\perp > 0.2$ GeV on all tracks causes essentially no loss of $D^*$ candidates.

In Fig. 1a the $\Delta M$ distribution for combinations with $1.80 < M(K\pi) < 1.92$ GeV is shown. A clear peak at the nominal value of $M(D^*) - M(D^0)$ [10] is observed. To determine the combinatorial background under the peak, combinations in the range $1.68 < M(K\pi) < 2.04$ GeV were used, in which both tracks forming the $D^0$ candidates had the same charge (these will be referred to as wrong charge combinations). The $\Delta M$ distribution from these combinations, normalized to the number of right charge combinations in the range $155 < \Delta M < 180$ MeV, is also shown in Fig. 1a.

The $M(K\pi)$ spectrum corresponding to combinations having a mass difference in the range $143 < \Delta M < 148\,\mathrm{MeV}$ is shown in Fig. 1b. A clear peak at the nominal $D^0$ mass of $1.8645 \pm 0.0005\,\mathrm{GeV}$ [10] is observed. The combinatorial background was again determined by using wrong charge combinations. The $M(K\pi)$ distribution from these combinations was normalized to the number of right charge combinations in the range $2.0 < M(K\pi) < 2.5\,\mathrm{GeV}$. A clear excess of right charge combinations with respect to the combinatorial background was observed for masses below that of the $D^0$ meson. This excess is reproduced by the MC simulation (when a sample including all decay modes of the $D^0$ is used), and is mainly due to events in which a $D^0$ decays into $K\pi\pi^0$ and the extra $\pi^0$ is not included in the $D^0$ invariant mass reconstruction.

The signals from Fig. 1 were fitted with the maximum likelihood method to a sum of a Gaussian (describing the signal) and a functional form (describing the background shape) of $A \cdot (\Delta M - m_\pi)^B$ for Fig. 1a and $\exp(C + D \cdot M(K\pi))$ for Fig. 1b. The mass and width values obtained were: $\Delta M = 145.44 \pm 0.08\,\mathrm{MeV}$, $\sigma = 0.68 \pm 0.08\,\mathrm{MeV}$ from Fig. 1a and $M(D^o) = 1860 \pm 4$ MeV, $\sigma = 29 \pm 4$ MeV from Fig. 1b. The mass values obtained are in agreement with the PDG values [10]. The width values agree with our MC simulations. The observed signals confirm that the reconstructed $D^*$ candidates come from channel (1). The contribution of other $D^o$ decay modes to this signal is negligible as estimated by MC studies. The number of reconstructed $D^*$'s was determined by subtracting the normalized background distributions described above from the right charge distributions. The use of a wider $M(K\pi)$ range for the wrong charge combinations compared with the signal region reduces the statistical error of the subtraction procedure. After subtracting the background from the $\Delta M$ distribution of Fig. 1a, a signal of $152 \pm 16$ reconstructed $D^*$'s was obtained, consistent with the corresponding subtracted signal from the $M(K\pi)$ distribution.

### 3.3 The $D^{*+} \to D^0\pi_S^+ \to (K^-\pi^+\pi^+\pi^-)\pi_S^+$ Decay Channel

For this channel, four tracks were combined to form a $D^0$ candidate. The invariant mass $M(K\pi\pi\pi)$ was calculated for combinations having a total charge of zero. Since no particle identification was used, kaon and pion masses were assumed in turn for each particle in the combination. A fifth track, assumed to be the soft pion, $\pi_S$, with a charge opposite to that of the kaon was added to the combination and the mass difference $\Delta M = M(K\pi\pi\pi\pi_S) - M(K\pi\pi\pi)$ was determined. Minimum transverse momenta of $0.5\,\mathrm{GeV}$ for the track taken to be the kaon and of $0.2\,\mathrm{GeV}$ for the other tracks were required.

Due to the higher number of decay particles in this channel, the combinatorial background is higher than that of channel (1). In order to achieve an improved signal to background ratio, we required the transverse momentum of the $K\pi\pi\pi\pi_S$ combination to be above $4\,\mathrm{GeV}$, and to satisfy the condition $p_\perp^{K\pi\pi\pi\pi_S} > 0.2 \cdot E_\perp^{\theta > 10^\circ}$. This latter requirement removed about one third of the combinatorial background, i.e. the contribution

from events with high $E_\perp^{\theta>10^\circ}$ in which a combination with relatively low transverse momentum was found. No reduction in the number of signal events was observed. Finally, the reconstructed $D^*$ candidates were required to be in the same pseudorapidity range as for channel (1), i.e. $-1.5 < \eta < 1.0$.

Fig. 2a shows the $\Delta M$ distribution for those combinations with $1.81 < M(K\pi\pi\pi) < 1.91\,\mathrm{GeV}$. The $M(K\pi\pi\pi)$ spectrum for combinations in the range $143 < \Delta M < 148\,\mathrm{MeV}$ is shown in Fig. 2b. A smaller window around the nominal $D^0$ mass was used in this channel because of the better mass resolution due to the lower average transverse momenta of the $D^0$ decay particles. The signals from Fig. 2 were fitted to a sum of a Gaussian (describing the signal) and a functional form (describing the background shape) of $A \cdot (\Delta M - m_\pi)^B$ for Fig. 2a and $P_2(x) = C + Dx + Ex^2$, where $x = M(K\pi\pi\pi)$ for Fig. 2b. The mass and width values obtained were: $\Delta M = 145.42 \pm 0.11$ MeV, $\sigma = 0.83 \pm 0.11$ MeV from Fig. 2a and $M(D^o) = 1859 \pm 3$ MeV, $\sigma = 19 \pm 3$ MeV from Fig. 2b. The mass values obtained are in agreement with the PDG values [10], and the widths agree with the MC values.

There are two main sources of background to the $D^*$ signals in this decay channel. The first one is the combinatorial background coming from events or tracks in which no $D^*$ decaying through this channel is produced. To determine this background, wrong charge combinations with total charge $\pm 2$ for the $D^0$ candidate and total charge $\pm 1$ for the $D^*$ candidate were used. The distributions of the wrong charge combinations were normalized to the number of right charge combinations for $\Delta M$ in the range $155 < \Delta M < 180\,\mathrm{MeV}$, and for $M(K\pi\pi\pi)$ in the range $2.0 < M(K\pi\pi\pi) < 2.5\,\mathrm{GeV}$ and are shown in Fig. 2. After the background subtraction, $199 \pm 29$ reconstructed $D^*$'s were observed in the $\Delta M$ distribution. The second source of background is due to events in which a $D^*$ decaying in this channel was produced, but more than one combination was reconstructed inside the signal region, due to the erroneous assignment of the kaon mass to a pion with the same charge from the $D^0$ decay. The fraction of $D^*$'s with a wrong $(K, \pi)$ mass assignment was found from MC calculations to be 16%. After subtracting this contribution, a final signal of $167 \pm 25$ reconstructed $D^*$'s was obtained. Monte Carlo studies show that the contribution of other $D^o$ decay modes to this signal is about 3% and was neglected.

# 4 Monte Carlo Simulation

The Monte Carlo programs PYTHIA [19] and a recent version of HERWIG [20, 21] containing an improved description of transverse energy distributions were used to model the hadronic final states in $c\bar{c}$ production and to study the efficiency of the data selection cuts. Both programs are general purpose event generators which include QCD LO matrix elements for charm photoproduction. They simulate higher order QCD radiation by parton shower evolution in the initial and final states, taking into account coherence effects from the interference of soft gluon amplitudes. Fragmentation into hadrons is simulated with a cluster algorithm [22] in the case of HERWIG, and with the LUND string model [23]

in the case of PYTHIA. In HERWIG, the lepton-photon vertex is calculated exactly for the direct photon processes and the equivalent photon approximation [24] is used for the resolved processes. In PYTHIA the Weizsäcker-Williams approximation [25] is used in both cases.

Large samples of $c\overline{c}$ events were generated with both MC programs. Direct and resolved photon events, including charm excitation, were generated using several parton distribution parametrizations for both the proton and the photon. The MRSG [26] parametrization for the proton and the GRV-G HO [27] for the photon were used to produce the reference samples. These samples had at least 20 times the statistics of the data, so their contribution to the statistical error was neglected. It was found from MC studies that, in the kinematic range used, the results are insensitive to contributions from charm excitation in the proton. However they are sensitive to charm excitation in the photon. The differences between results obtained with and without charm excitation in the photon are included in the systematic errors. A large sample of $b\overline{b}$ events was also generated with PYTHIA to allow an estimation of the fraction of photoproduced $D^*$'s originating from this process.

Events containing at least one charged $D^*$ decaying into channel (1) or (2) were processed through the standard ZEUS detector and trigger simulation programs and through the event reconstruction package.

# 5 Cross Section Determination

The integrated $D^*$ electroproduction cross section in the kinematic region defined by the selection cuts $Q^2 < 4\,\mathrm{GeV}^2$, $115 < W < 280\,\mathrm{GeV}$, $-1.5 < \eta^{D^*} < 1.0$ and $p_\perp^{D^*} > 3$ or $4\,\mathrm{GeV}$ is calculated using the formula:

$$\sigma_{ep\to D^*X} = \frac{N_{corr}^{D^*}}{\mathcal{L}\cdot Br},$$

where $N_{corr}^{D^*}$ is the acceptance-corrected number of $D^*$, $Br$ is the combined branching ratio of a given channel (see Table 1) and $\mathcal{L} = 2.99 \pm 0.05\,\mathrm{pb}^{-1}$ is the integrated luminosity.

The usual method to correct data by the ratio of generated to reconstructed MC events is valid when the MC well describes the data distributions of quantities used in the analysis. In our case most of these distributions are well described by the MC events. However, for the $E_\perp^{\theta>10^\circ}$ distribution the data yield higher values compared to the events simulated with PYTHIA. Therefore the reference MC used to calculate the acceptance for channel (1) was HERWIG. In the case of channel (2) PYTHIA was used since HERWIG does not reproduce the decay width of the resonances, and hence does not describe correctly the $D^0$ decays into four particles.

In order to minimize the MC dependence of the corrections for the $E_\perp^{\theta>10^\circ}$ cut in both channels, a two step procedure was used to calculate $N_{corr}^{D^*}$:

(a) A weighting factor $\omega_1$ was obtained from the MC simulation and applied to each reconstructed $D^*$ candidate. These events were corrected for the tracking efficiency of the $D^*$ reconstruction algorithm and for all trigger and event selection cuts except for the $E_\perp^{\theta>10^\circ}$ cut. The factor $\omega_1$ is defined as the number of generated $D^*$'s divided by the number of reconstructed $D^*$'s. It is calculated in a three-dimensional grid in the reconstructed quantities $p_\perp^{D^*}$, $\eta^{D^*}$ and $W_{\mathsf{JB}}$. The average values of $\omega_1$ are $2.99 \pm 0.03$ and $3.07 \pm 0.04$ for channel (1) and channel (2), respectively. The variation of $\omega_1$ as a function of any of the three grid variables is less than a factor of two in the restricted kinematic range.

(b) To calculate the correction for the $E_\perp^{\theta>10^\circ} > 12\,\mathrm{GeV}$ cut we used an independent $D^*$ data sample selected for channel (1) with no cut on the energy deposition in the calorimeter at the TLT. Only tracking information was used for this sample selection at the TLT. The corresponding correction factor $\omega_2$ is given by the total number of $D^*$'s (corrected as in (a) above) obtained with the TLT tracking selection divided by the number of those $D^*$'s (corrected as in (a) above) in events which satisfy the cut $E_\perp^{\theta>10^\circ} > 12\,\mathrm{GeV}$. The correction by this method increases the statistical error of the result, but reduces the systematic error due to the different MC modeling of the $E_\perp^{\theta>10^\circ}$ distribution. The factor $\omega_2$ was applied as an overall weight for the total cross section calculation or bin-by-bin in each differential cross section distribution. Since the $\omega_2$ correction is independent of the tracking acceptance (which is included in $\omega_1$), the $\omega_2$ weights of channel (1) were used also for the $N_{corr}^{D^*}$ evaluation of channel (2). The average values of $\omega_2$ are $1.8 \pm 0.2$ and $1.4 \pm 0.1$ for $p_\perp > 3\,\mathrm{GeV}$ and $p_\perp > 4\,\mathrm{GeV}$, respectively.

The reconstructed number of $D^*$ mesons after background subtraction ($N_{meas}^{D^*}$), the acceptance corrected number of produced $D^*$'s ($N_{corr}^{D^*} = \omega_1\omega_2 N_{meas}^{D^*}$), the branching ratios $Br$ [10] and the integrated cross sections for both decay channels are presented in Table 1. For comparison with channel (2), the value obtained for channel (1) requiring $p_\perp^{D^*} > 4\,\mathrm{GeV}$ is also shown. The cross sections of both channels are in good agreement for the same kinematic region.

The differential cross sections $d\sigma/dp_\perp^{D^*}$, $d\sigma/d\eta^{D^*}$ and $d\sigma/dW$ were calculated using the same correction procedure in five bins in $p_\perp^{D^*}$ (3-4; 4-5; 5-6; 6-8; 8-12 GeV), three bins in $\eta^{D^*}$ ((-1.5)-(-0.6); (-0.6)-(0.1); (0.1-1.0)) and three bins in $W$ (115-170; 170-225; 225-280 GeV). For each variable ($p_\perp^{D^*}$, $\eta^{D^*}$, $W$), the other two variables are integrated over their kinematic region. The combinatorial background was subtracted bin-by-bin from each distribution using the method described in section 3. The $d\sigma/dp_\perp^{D^*}$ distributions for both channels (1) and (2) are shown in Fig. 3. The $d\sigma/d\eta^{D^*}$ and $d\sigma/dW$ distributions for channel (1) are shown in Fig. 4. The results are in agreement with those of the H1 untagged photoproduction data [7], also shown in Fig. 3, with the same $D^*$ rapidity range and with $95 < W < 268$ GeV, which is quite similar to the kinematic range of this measurement.

| Channel | $p_\perp^{D^*}$(GeV) | $N_{meas}^{D^*}$ | $N_{corr}^{D^*}$ | $Br$ | $\sigma_{ep\to D^*X}$ (nb) |
|---|---|---|---|---|---|
| (1) | $> 3$ | $152 \pm 16$ | $828 \pm 129$ | $0.0262 \pm 0.0010$ | $10.6 \pm 1.7 \pm^{1.6}_{1.3}$ |
| (1) | $> 4$ | $97 \pm 11$ | $348 \pm 53$ | $0.0262 \pm 0.0010$ | $4.5 \pm 0.7 \pm 0.6$ |
| (2) | $> 4$ | $167 \pm 25$ | $739 \pm 128$ | $0.051 \pm 0.003$ | $4.8 \pm 0.8 \pm^{1.0}_{0.6}$ |

Table 1: Cross section $\sigma_{ep\to D^*X}$ and related quantities for $Q^2 < 4$ GeV$^2$, $115 < W < 280$ GeV and $-1.5 < \eta^{D^*} < 1.0$ .

## 5.1 Systematic Uncertainties

A detailed study of possible sources of systematic uncertainties was carried out, which we now summarize.

Trigger acceptance uncertainties are mainly due to the different energy distributions predicted by the two event generators PYTHIA and HERWIG with and without flavour excitation. The uncertainties were determined from the difference between the cross sections obtained with both MC generators. For channel (1) the largest shift was $-11\%$. For channel (2) the largest shift was $+10\%$.

To estimate the uncertainties in the tracking procedure, all track selection cuts were varied. In the present analysis only tracks associated with the event vertex were considered. The systematic error due to any $D^*$ track not being fitted to the vertex was estimated from a careful comparison of vertex fitting in data and Monte Carlo. The resulting uncertainties on the cross sections are $^{+14}_{-4}\%$ and $^{+18}_{-10}\%$ for channels (1) and (2), respectively.

The uncertainty in the acceptance of the $E_\perp^{\theta>10^\circ} > 12$ GeV cut was estimated by changing the cut value by $\pm 0.5$ GeV. A variation in the cross section of $^{+4}_{-0}\%$ for channel (1) and $^{+3}_{-7}\%$ for channel (2) was found. A shift of $\pm 3\%$ in the calorimeter energy scale produces a variation of $^{+2}_{-0}\%$ for channel (1) and $^{+0}_{-1}\%$ for channel (2).

Background estimation uncertainties were determined by varying the normalization region. The uncertainties were found to be $^{+0}_{-1}\%$ for both channels (1) and (2).

The parton density parametrizations [28] MRS(G), MRS(A'),GRV94 HO and CTEQ3M for the proton and GRV-G HO, GRV-G LO, LAC-G1, GS-G HO and DG-G1 for the photon were used in the MC event simulation. No significant variation of the acceptance was found in the kinematic region used for this analysis.

Finally, contributions of $\pm 1.5\%$ from the luminosity measurement, and $\pm 3.7\%$ or $\pm 5.7\%$ from the branching ratios [10] of channels (1) or (2) respectively, were included.

All contributions to the systematic errors were added in quadrature. The final systematic errors to the total cross sections are given in table 1. For the differential cross sections they were added in quadrature to the statistical errors and are indicated as the outer error bars in Figures 3 and 4.

# 6 Comparison with NLO QCD Calculations

Full NLO computations of differential cross sections for heavy quark production in any kinematic region [3, 9] became available recently. We compare our measurements with two such calculations.

One of the two computations was done in the massive charm scheme [3], where $m_c$ acts as a cutoff for the perturbative calculation. The program for $c\overline{c}$ photoproduction [29] from this computation was used to produce total and differential $D^*$ cross sections in the restricted kinematic region of our measurement. From MC studies it was found that the contribution of $b\overline{b}$ production to the $D^*$ cross section is below 5%. The charm fragmentation into $D^*$ was performed using the Peterson formula [30]:

$$f(z) \propto \left[ z \left( 1 - \frac{1}{z} - \frac{\epsilon_c}{(1-z)} \right)^2 \right]^{-1},$$

with $\epsilon_c = 0.06$ [31] and using the branching ratio $Br(c \to D^{*+}) = 0.260 \pm 0.021$ as measured by the OPAL collaboration [32]. Here $z$ is the fraction of the charm quark momentum taken by the $D^*$. In order to convert the photoproduction differential cross sections into electroproduction cross sections, the $W$ range from 115 to 280 GeV was divided into 15 GeV wide bins. The photoproduction cross sections were calculated in the center of each bin and the results were added after multiplying by the proper flux factors [6].

A reference calculation was performed with the MRSG and GRV-G HO parton density parametrizations for the proton and photon, respectively. The renormalization scale used was $\mu_R = m_\perp = \sqrt{m_c^2 + p_\perp^2}$ ($m_c = 1.5$ GeV) and the factorization scales of the photon and proton structure functions was $\mu_F = 2\mu_R$. The predicted reference cross sections thus obtained are compared to the measured ones in Figures 3 and 4. Varying $m_c$ between 1.2–1.8 GeV or $\mu_R$ between 0.5–2.0$m_\perp$ changes the cross sections in our kinematic range within $\pm 20\%$. Decreasing $\epsilon_c$ to 0.035 [32] increases the cross section by 15%. Using different proton or photon parton density parametrizations changes the cross section by less than 10%. All of the cross sections predicted by [3] using the reference parameters are lower than the data and the cross section in the kinematic region of the $K\pi$ channel is about 50% of the measured one. Better agreement with the data can be obtained with the choice of the parameters $\mu_R = 0.5\, m_\perp$ and $m_c = 1.2$ GeV as shown in Figures 3 and 4. With the present statistics the shapes of the NLO predictions are in reasonable agreement with the data.

Recently, another type of NLO calculation [9] was compared to the H1 and ZEUS preliminary results. In this approach the charm quark is treated according to the massless factorization scheme, which assumes charm to be one of the active flavours inside the proton and the photon, in contrast to the massive charm scheme. The differential distributions obtained with the massless approach NLO calculation are shown in Figures 3 and 4. The parton density parametrizations used for the proton and photon were CTEQ4M [33] and GRV HO [27], respectively. The renormalization and factorization scales, as well as the values of $m_c$ and $\epsilon_c$ used are the same as in the reference calculation of the massive-charm approach. The agreement with our data is good. Using a different proton parametrization (MRSG [26]) hardly changes the results [9] while the photon parametrization ACFGP-mc [34] reduces the cross section by 20% in our kinematic range [35].

# 7 Summary

The integrated and differential $D^*$ photoproduction cross sections in $ep$ collisions at HERA have been measured with the ZEUS detector in the restricted kinematic region $Q^2 < 4\,\mathrm{GeV}^2$, $115 < W < 280\,\mathrm{GeV}$, $p_\perp^{D^*} > 3\,\mathrm{GeV}$ and $-1.5 < \eta^{D^*} < 1.0$. The cross section $\sigma_{ep\to D^* X}$ obtained using the channel $D^{*+} \to D^0\pi_S^+ \to (K^-\pi^+)\pi_S^+$ was measured to be $(10.6 \pm 1.7(stat.)\,^{1.6}_{1.3}\,(syst.))\,\mathrm{nb}$. Another $D^*$ decay channel, $D^{*+} \to D^0\pi_S^+ \to (K^-\pi^+\pi^+\pi^-)\pi_S^+$, has been studied and good agreement with the $K\pi$ channel has been found in the region of overlap ($p_\perp^{D^*} > 4\,\mathrm{GeV}$). A NLO perturbative QCD massive charm scheme calculation predicts cross sections smaller than our measured values. Another NLO calculation in which the charm quark is treated according to the massless factorization scheme is in agreement with the data. The shapes of the differential cross sections $d\sigma/dp_\perp^{D^*}$, $d\sigma/d\eta^{D^*}$ and $d\sigma/dW$ are reasonably reproduced by both models.

# Acknowledgments

The experiment was made possible by the inventiveness and the diligent efforts of the HERA machine group who continued to run HERA most efficiently during 1994. The design, construction and installation of the ZEUS detector has been made possible by the ingenuity and dedicated effort of many people from inside DESY and from the home institutes, who are not listed as authors. Their contributions are acknowledged with great appreciation. We thank M. Cacciari, S. Frixione, B.A. Kniehl and G. Kramer for discussions and S. Frixione for providing us with the NLO code. The strong support and encouragement of the DESY Directorate has been invaluable. We also gratefully acknowledge the support of the DESY computing and network services.

# References


[1] R.K. Ellis and P. Nason, Nucl. Phys. B 312 (1989) 551;
P. Nason, S. Dawson and R.K. Ellis, Nucl. Phys. B 303 (1988) 607;
J. Smith and W.L. van Neerven, Nucl. Phys. B 374 (1992) 36.

[2] S. Frixione et al. Phys. Lett. B 348 (1995) 633;
S. Frixione et al. Nucl. Phys. B 431 (1994) 453.

[3] S. Frixione et al. Nucl. Phys. B 454 (1995) 3.

[4] B.A. Kniehl et al., Phys. Lett. B 356 (1995) 539.

[5] M. Cacciari and M. Greco, Z. Phys. C 69 (1996) 459.

[6] ZEUS Collaboration, M. Derrick et al., Phys. Lett. B 349 (1995) 225.

[7] H1 Collaboration, S. Aid et al., Nucl. Phys. B 472 (1996) 32,
and C. Grab, private communication.

[8] V.A. Saleev and N.P. Zotov, Mod. Phys. Lett. A 11 (1996) 25;
hep-ph/9610346 (1996).

[9] B.A. Kniehl, G. Kramer and M. Spira, DESY 96-210, hep-ph/9610267 (1996).

[10] R.M. Barnett et al., Particle Data Group, Phys. Rev. D 54 (1996) 1.

[11] S. Nussinov, Phys. Rev. Lett. 35 (1975) 1672;
G.J. Feldman et al., Phys. Rev. Lett. 38 (1977) 1313.

[12] The ZEUS Detector Status Report 1993, DESY 1993.

[13] ZEUS Collaboration, M. Derrick et al., Phys. Lett. B 293 (1992) 465.

[14] N. Harnew et al., Nucl. Instr. Meth. A 279 (1989) 290;
C.B. Brooks et al., Nucl. Instr. Meth. A 283 (1989) 477;
B. Foster et al., Nucl. Phys. B (Proc. Suppl.) 32 (1993) 181;
B. Foster et al., Nucl. Instr. Meth. A 338 (1994) 254.

[15] M. Derrick et al., Nucl. Instr. Meth. A 309 (1991) 77;
A. Andresen et al., ibid. A 309 (1991) 101;
A. Caldwell et al., ibid. A 321 (1992) 356;
A. Bernstein et al., ibid. A 336 (1993) 23.

[16] J. Andruszkòw et al., DESY 92-066 (1992);
ZEUS Collaboration, M. Derrick et al., Z. Phys.C 63 (1994) 391.

[17] ZEUS Collaboration, M. Derrick et al., Phys. Lett. B 322 (1994) 287.

[18] F. Jacquet and A. Blondel, Proc. of the Study for an *ep* Facility for Europe, ed. U.Amaldi, DESY 79/48 (1979) 377.

[19] T. Sjöstrand, Comp. Phys. Comm. 82 (1994) 74.

[20] G. Marchesini et al., Comp. Phys. Comm. 67 (1992) 465.

[21] G. Abbiendi, M. Seymour, private communication.

[22] B. R. Webber, Nucl. Phys. B238 (1984) 492.

[23] B. Andersson et al., Phys. Rep. 97 (1983) 31.

[24] V.M. Budnev et al., Phys. Rep. 15 (1975) 181.

[25] C.F. Weizsäcker, Z. Phys. 88 (1934) 612;
E.J. Williams, Phys. Rev. 45 (1934) 729.

[26] A.D. Martin, W.J. Stirling and R.G. Roberts, Phys. Lett. B 354 (1995) 155.

[27] M. Glück, E. Reya and A. Vogt, Phys. Rev. D 46 (1992) 1973.

[28] H. Plothow-Besch, Int. J. Mod. Phys. A10 (1995) 2901.

[29] S. Frixione et al. Nucl. Phys. B 412 (1994) 225;
M.L. Mangano et al. Nucl. Phys. B 373 (1992) 295.

[30] C. Peterson et al., Phys. Rev. D 27 (1983) 105.

[31] J. Chrin, Z. Phys. C 36 (1987) 163.

[32] OPAL Collaboration, R.Akers et al., Z. Phys. C 67 (1995) 27.

[33] H.L. Lai et al., MSUHEP-60426, CTEQ-604 and hep-ph/9606399 (1996).

[34] P. Aurenche et al., Z. Phys. C 56 (1992) 589.

[35] B.A. Kniehl, G. Kramer, private communication.

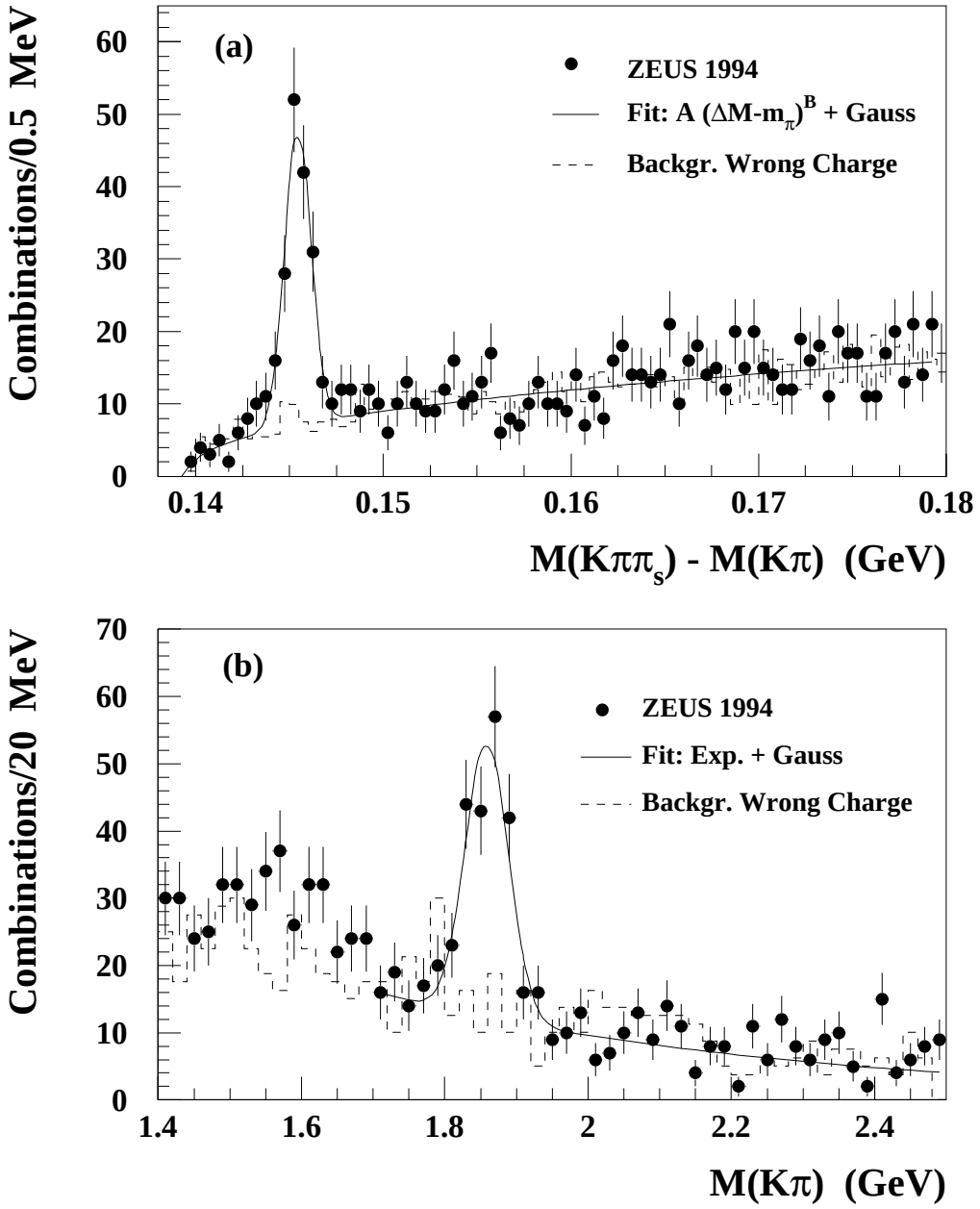


Figure 1: $\Delta M$ and $M(K\pi)$ distributions for channel (1). In (a), the $\Delta M$ distributions for right charge combinations from the $M(K\pi)$ signal region (full circles) and for wrong charge combinations from the region $1.68 < M(K\pi) < 2.04\,\mathrm{GeV}$ (dashed histogram) are shown. In (b), the $M(K\pi)$ distributions for the right charge combinations from the $\Delta M$ signal region (full circles) and for wrong charge combinations from the $\Delta M$ signal region (dashed histogram) are shown. The full lines are the results of fits to a sum of a Gaussian and the functional form $A \cdot (\Delta M - m_\pi)^B$ for (a) and $\exp(C + D \cdot M(K\pi))$ for (b).

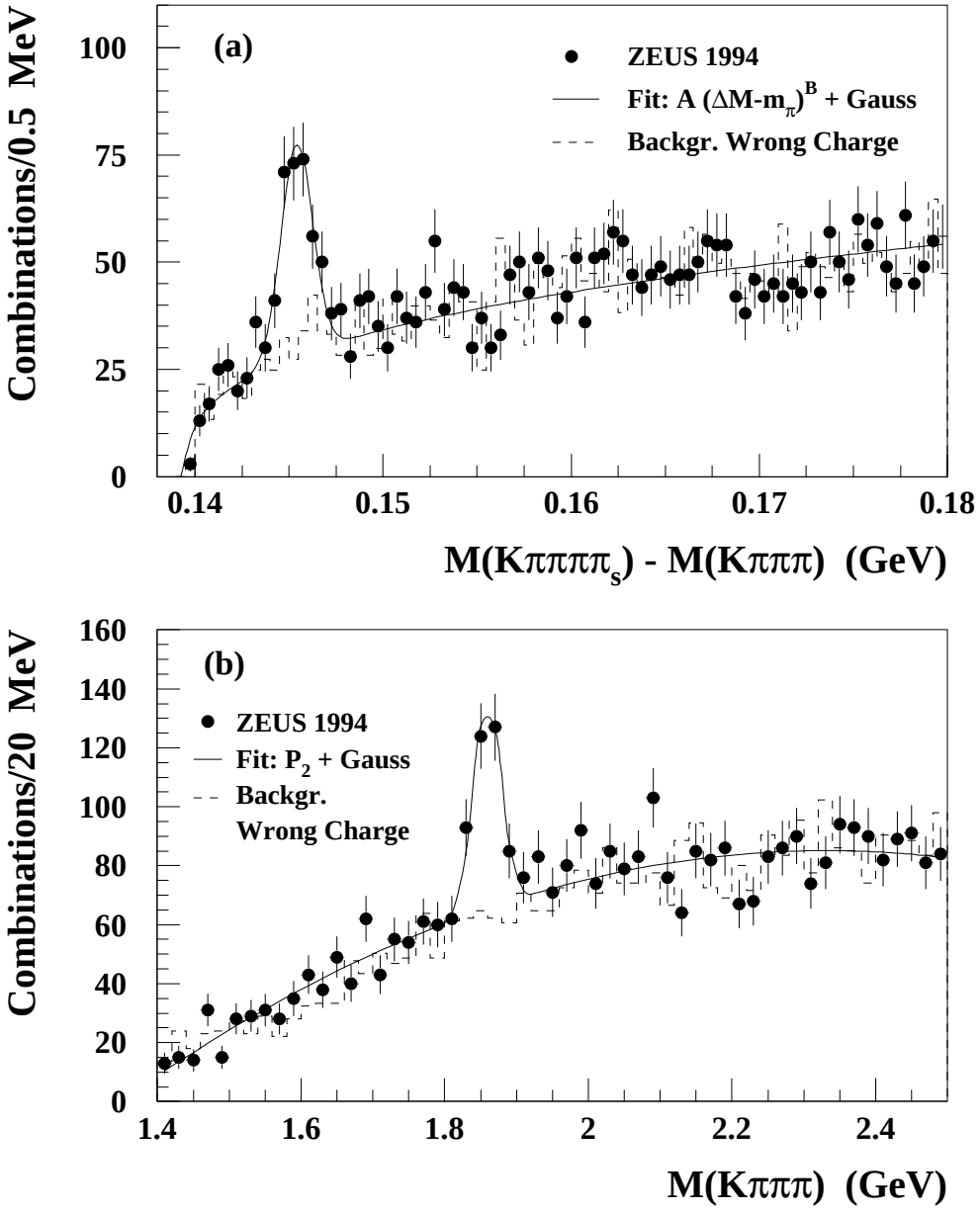


Figure 2: $\Delta M$ and $M(K\pi\pi\pi)$ distributions for channel (2). In (a), the $\Delta M$ distributions are shown for the right charge combinations from the $M(K\pi\pi\pi)$ signal region (full circles), and for the background estimate using the wrong charge combinations (dashed histogram) as described in the text. In (b), the $M(K\pi\pi\pi)$ distributions are shown for the right charge combinations from the $\Delta M$ signal region (full circles) and for the background estimate using the wrong charge combinations (dashed histogram) as described in the text. The full lines are the results of fits to a sum of a Gaussian and the functional form $A\cdot(\Delta M - m_\pi)^B$ for (a) and $P_2(x) = C + Dx + Ex^2$, where $x = M(K\pi\pi\pi)$ for (b).

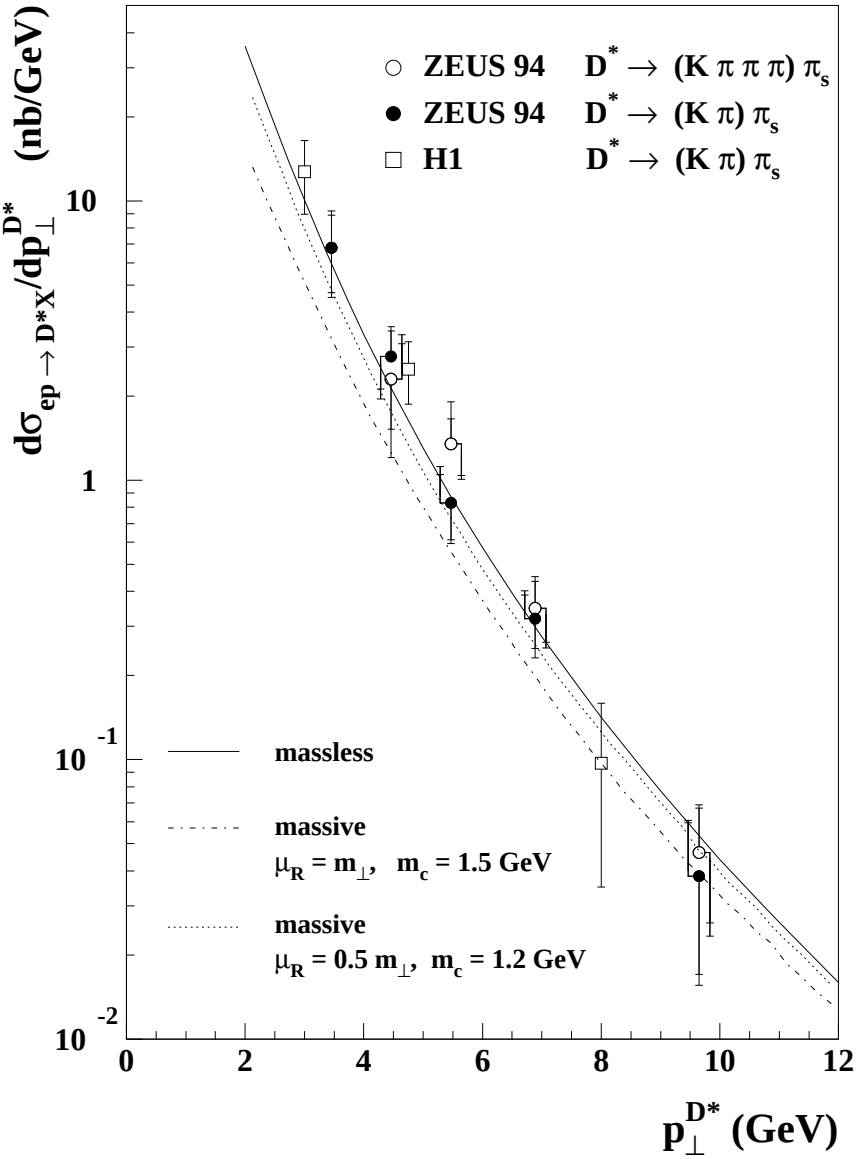


Figure 3: The differential cross section $d\sigma_{ep\to D^*X}/dp_\perp^{D^*}$ of $D^*$ photoproduction, $Q^2 < 4\,\mathrm{GeV}^2$, in the kinematic region $115 < W < 280\,\mathrm{GeV}$ and $-1.5 < \eta^{D^*} < 1.0$. The experimental points are drawn at the positions of the average values of an exponential fit in each bin. The inner part of the vertical error bars shows the statistical error, while the outer one shows the statistical and systematic errors added in quadrature. The H1 points [7] include statistical errors and systematical errors due to trigger efficiency. The prediction of a NLO perturbative QCD calculation from a massive charm approach [3] is given by the dot-dashed curve, using MRSG and GRV-G HO as parton density parametrizations for the proton and photon respectively, fragmentation parameter $\epsilon_c = 0.06$, renormalization scale $\mu_R = m_\perp$ and $m_c = 1.5\,\mathrm{GeV}$. The dotted curve is from the same calculation, but for $\mu_R = 0.5\,m_\perp$ and $m_c = 1.2\,\mathrm{GeV}$. The full curve comes from the massless charm approach calculation [9], using the same parameters as for the dot-dashed curve, but with CTEQ4M taken for the parton density parametrization for the proton.

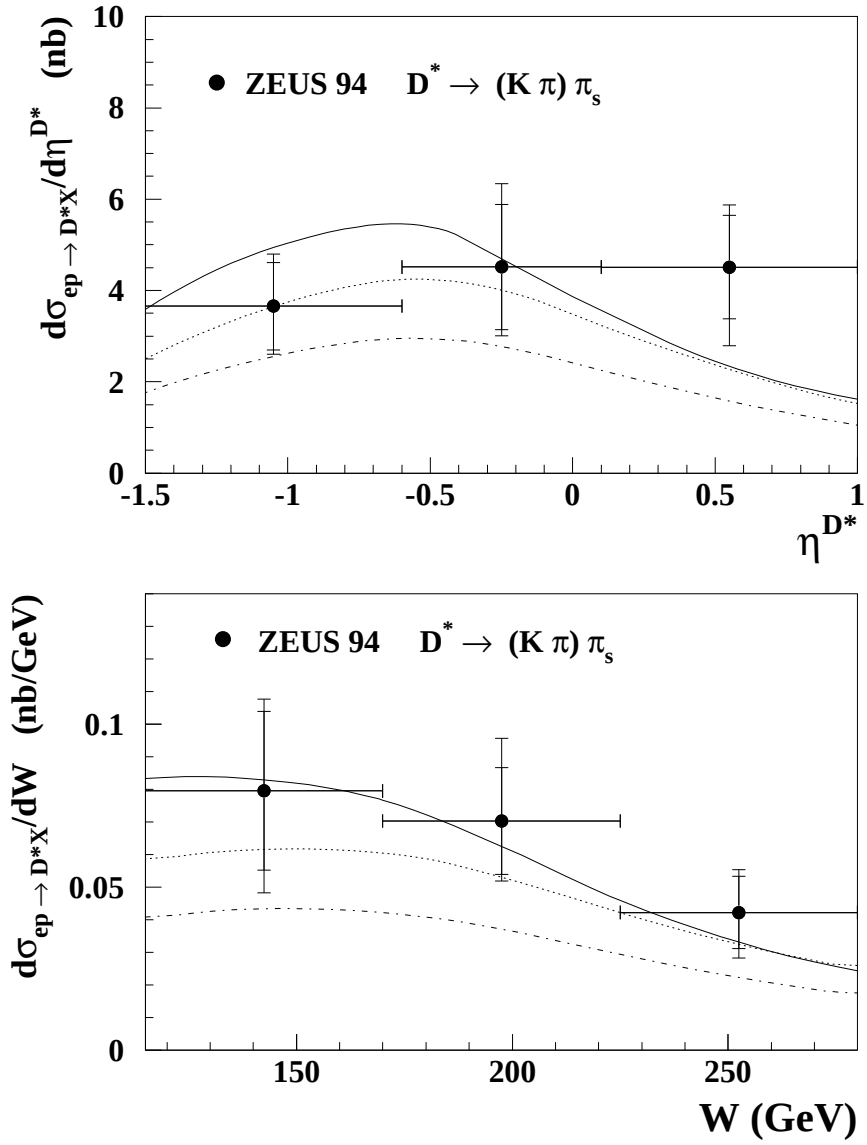


Figure 4: Differential cross sections for $Q^2 < 4\,\mathrm{GeV}^2$ : $d\sigma_{ep\to D^*X}/d\eta^{D^*}$ in the kinematic region $115 < W < 280\,\mathrm{GeV}$ and $p_\perp^{D^*} > 3\,\mathrm{GeV}$ (upper plot) and $d\sigma_{ep\to D^*X}/dW$ in the kinematic region $p_\perp^{D^*} > 3\,\mathrm{GeV}$ and $-1.5 < \eta^{D^*} < 1.0$ (lower plot) for channel (1). The points are drawn at the centres of the corresponding bins. The inner part of the vertical error bars shows the statistical error, while the outer one shows the statistical and systematic errors added in quadrature. The prediction of a NLO perturbative QCD calculation from a massive charm approach [3] is given by the dot-dashed curve, using MRSG and GRV-G HO as parton density parametrizations for the proton and photon respectively, fragmentation parameter $\epsilon_c = 0.06$, renormalization scale $\mu_R = m_\perp$ and $m_c = 1.5\,\mathrm{GeV}$. The dotted curve is from the same calculation, but for $\mu_R = 0.5\,m_\perp$ and $m_c = 1.2\,\mathrm{GeV}$. The full curve comes from the massless charm approach calculation [9], using the same parameters as for the dot-dashed curve, but with CTEQ4M taken for the parton density parametrization for the proton.